Journal of
Synchrotron
Radiation

ISSN 1600-5775

Received 19 August 2013
Accepted 20 November 2013

A compact synchrotron-based transmission X-ray microscope

Yu-Sheng Chen,[a] Huang-Han Chen,[a] Tsong-Tse Li,[a] Edwin Ong,[a] Jun Lim,[b] Giorgio Margaritondo,[c] En-Te Hwu[a]* and Yeukuang Hwu[a]*

[a]Institute of Physics, Academia Sinica, 128 Academia Road, Taipei 115, Taiwan, [b]Pohang Light Source, Pohang University of Science and Technology, Pohang 790-784, Republic of Korea, and [c]School of Basic Science, Ecole Polytechnique Fédérale de Lausanne, Lausanne 1015, Switzerland. *E-mail: whoand@phys.sinica.edu.tw, phhwu@sinica.edu.tw

A compact transmission X-ray microscope has been designed and implemented based on a cylindrical symmetry around the optical axis that sharply limits the instabilities due to thermal mechanical drift. Identical compact multi-axis closed-loop actuation modules drive different optical components. The design is modular and simplifies the change of individual parts, *e.g.* the use of different magnification and focusing devices. This compact instrument can be easily transported between laboratory and synchrotron facilities and quickly put into operation. An automated alignment mechanism simplifies the assembly of different modules after transportation. After describing the design details, the results of the first tests are presented.

Keywords: X-ray microscopy; Fresnel zone plate; nanopositioning; thermal stability.

1. Introduction

Recent technical progress has greatly improved the performances of transmission X-ray microscope (TXM) instruments, notably the space resolution (Yin *et al.*, 2006; Feng *et al.*, 2007; Wojcik *et al.*, 2010; Kuwabara *et al.*, 2011; Uhlén *et al.*, 2011; David *et al.*, 2011; Gorniak *et al.*, 2011; Gorelick *et al.*, 2011; Kagoshima *et al.*, 2011; Chubarova *et al.*, 2011; Mayer *et al.*, 2011; Koyama *et al.*, 2012; Berujon *et al.*, 2012; Nilsson *et al.*, 2012; Chao *et al.*, 2012; Rehbein *et al.*, 2012; Chu *et al.*, 2008; Chen *et al.*, 2008, 2011), opening up entirely new application domains of this powerful technique. However, the technical problems are far from being entirely solved. We present here a new instrument that tackles two of the most critical ones: the transfer to and from synchrotron beamlines and thermal instabilities that affect the ultimate performances. The instrument could actually be suitable for use with non-synchrotron X-rays sources, further expanding its possible applications.

The size, weight and fragility of standard X-ray microscopes are indeed critical issues. A typical TXM instrument, for example, occupies a large optical table (normally 2 m long) that is not easy to transport. Putting the instrument into operation after transport to a beamline is a delicate and lengthy operation.

Thermal instabilities due to drifts in the local temperature are another critical problem. A standard TXM has a low-symmetry design with respect to the optical axis, in which different optical components are driven by actuators of different size and shape. As the local temperature varies, the thermal expansion of such actuators causes variations on the scale of hundredths of micrometers, with an important impact on instruments that now reach resolution levels of 10–20 nm (Chen *et al.*, 2011; Chien *et al.*, 2013; Wu, Hwu & Margaritondo, 2012; Wu, Chen *et al.*, 2012). Specifically, thermal instabilities can blur the images on a scale of a few minutes, affecting the resolution in many types of studies.

Fig. 1(*a*) shows a standard actuation system for the optical components of a TXM, in this case a pinhole. The three directional (X, Y, Z) actuators are stacked on the optical table; the typical total height is 150 mm, thus a 1 K temperature increase changes it by a few micrometers (based on the 17.3×10^{-6} m mK^{-1} and 22×10^{-6} m mK^{-1} linear thermal expansion coefficients of 304 stainless steel and aluminium). The standard TXM design places actuators for different optical components in different orientations to avoid mechanical

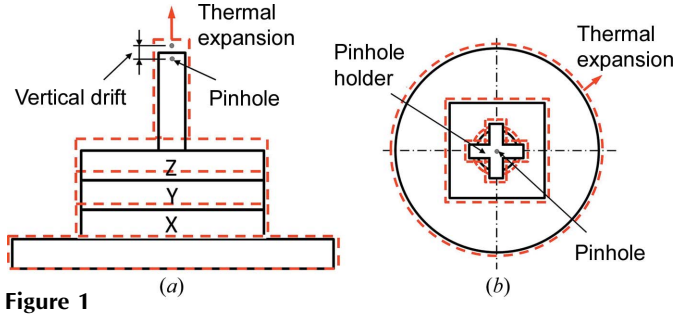

Figure 1
(*a*) Schematic front view of the actuator design for a pinhole model in a standard X-ray microscope. (*b*) Similar schematic view of our symmetric actuator design.

interference: this, however, induces thermal drifts in different directions. TXM is now moving towards the 10 nm resolution level, but no standard instruments design is compatible with that objective, without extreme control of the local temperature.

Our design deals with both of the above problems. For thermal instability, a component like a pinhole, mounted on an actuator, is placed along the optical axis as shown in Fig. 1(*b*). This automatically reduces the effects of thermal expansion since the component remains along the axis. However, the thermal expansion of the support posts must also be minimized. In the most recent version of our instrument, this was achieved by replacing the previously used aluminium posts with low-expansion Invar modules.

The design with high symmetry with respect to the optical axis is a key feature of our instruments. Another key feature is that the actuators for all optical components are identical. This results in a modular design that makes it possible to change the instrument components with minimal interference on the alignment of other components. For example, the magnifying element can be easily changed, *e.g.* from a zone plate to a capillary system and *vice versa*. In general terms, putting the components along the optical axis simplifies all alignment operations.

In addition, the use of identical design for all components reduces the effects of relative movements due to different thermal expansion. This complements the benefits of using a symmetric design.

2. Design of the multi-axis actuation module

The design adopted for all multi-axis actuation modules of our TXM (see Fig. 2) has a thickness of 21 mm and a diameter of 140 mm. The module (Fig. 2*a*) includes the *X*, *Y* and *Z* actuators with central circular opening of 20 mm. Each actuator is driven by a piezo stack and the moving range for each direction can reach 12.5 mm. A stick-slip mechanism (Niedermann *et al.*, 1988) drives the actuator for coarse motion, 30 nm per step, whereas the fine-motion piezo stack delivers sub-nanometer positioning accuracy (patent pending: US 2013/0188249A1).

The position feedback is provided by an optical encoder (Mercury II 6000, MicroE system) for each direction, reaching a 1.2 nm accuracy. The actuator module, as seen in Fig. 2(*b*), also provides the control of the angular position as required; for example, for the sample holder when working in a tomographic mode. The rotational motion is also driven by a piezo system, and is monitored by an angular sensor (Ceramic sensor model 59579, Applied Geomechanics) with a range and resolution of $\pm 80^\circ$ and 0.001°, respectively.

Fig. 3 shows our TXM, with two parts connected by carbon fiber tubes. The first part includes the optical components processing the X-ray beam plus the sample stage. The second part includes the X-ray imaging system (scintillator, visible lens and visible detector); its components can be moved longitudinally. The carbon fiber tubes (38 mm diameter) have low weight and high rigidity. The total length can be adjusted by using different combinations of individual segments; this is required, for example, when using different zone plates for different resolution and magnification.

Overall, the first part of the TXM (see Fig. 4) includes seven identical actuator modules, for the condenser, the pinhole, the sample holder, the magnifying lens (*e.g.* a zone plate), the

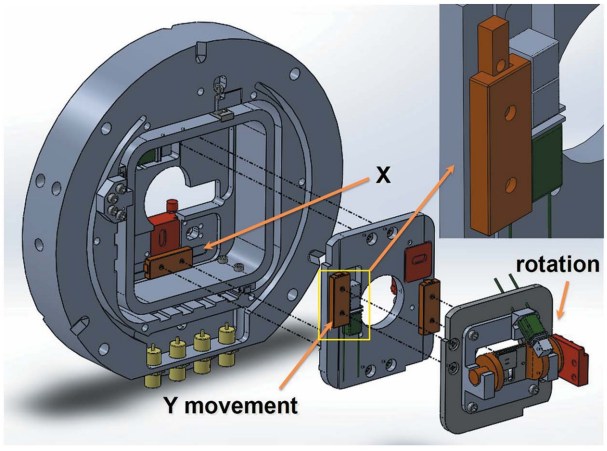

(*a*)

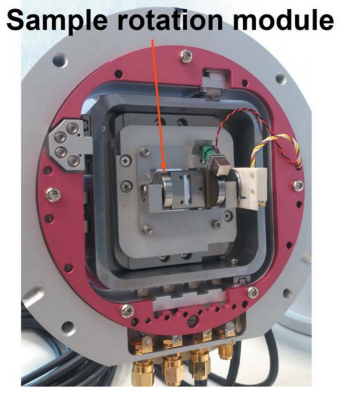

(*b*)

Figure 2
(*a*) Schematic three-dimensional drawing of the design of an actuation module, almost identical for all modules of the TXM. The different components of the module are shown separated from each other. (*b*) Photograph of the rotation module.

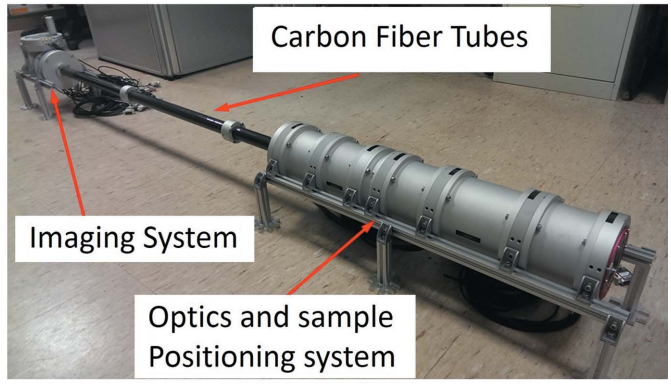

Figure 3
Overall view of the entire TXM system. The total length is approximately 2 m.

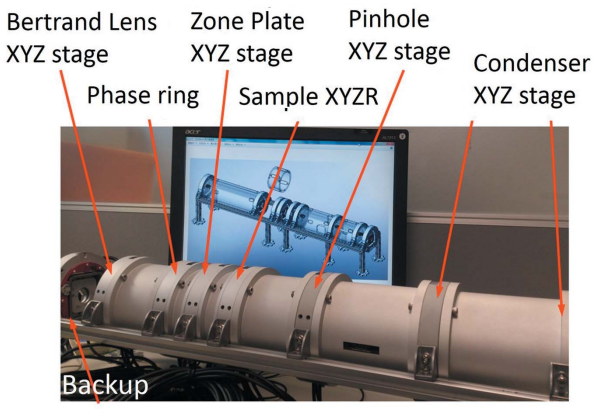

Figure 4
Photograph of the upstream part of the TXM system, showing the position of the different modules.

phase ring and the Bertrand lens. Between adjacent actuation modules there are spacing barrels that can be filled with different gases or left under vacuum. A kinematic coupling mechanism for each barrel provides automatic coarse alignment between actuation modules, barrels and the optical axis.

Fig. 5 shows details of the X-ray imaging system. Note that this system is much less sensitive to thermal drifts than the X-ray adjustment and sample scanning modules. In this case, thermal drift can only cause small and easily correctable image shifts. Even so, we did use the same mechanisms as for the actuators to achieve a uniform design, as seen in Fig. 5.

3. Test results

This compact TXM system was assembled and successfully tested in the BL 7C XNI beamline of Pohang Light Source II (PLS-II), Korea. The beamline provides X-ray photons from a 20 mm-period 70 pole undulator and a double-crystal monochromator. Photon energy is set at 6.5 keV for this test. A glass capillary condenser (Huang & Bilderback, 2006) was placed immediately upstream of the specimen to provide the necessary cone illumination. An image field of view of ~20 μm × 20 μm is magnified by the Au Fresnel zone plate objectives (50 nm outermost zone and 900 nm thickness) (Lo *et al.*, 2007; Chen *et al.*, 2008*b*) before reaching the imaging system ~1.5 m away from the objective. The imaging detecting system consists of a 20 μm-thick Tb:LSO scintillator, a 20× visible-light objective and a CCD (4096 × 4096 pixels, Alta U series, Apogee Instruments). With the 200 mA electron beam current of PLS-II operated in top-up mode of constant current, an image can be acquired in <1 s.

The thermal stability of the instrument was first assessed by monitoring the position of nominally fixed points of different modules as a function of time. The measurements were conducted with laser interferometry. The results systematically demonstrated position changes of less than 200 nm, stabilized within minutes, and a long-term drift afterwards of less than 100 nm over a time up to one day or more (Hwu *et al.*, 2013). The impact of thermal stability on the performances was then assessed by imaging a standard star test pattern. The recording time was of the order of tens of seconds per image and images were recorded over periods of several minutes. Fig. 6(*a*) shows a cumulative X-ray image, a sum of the individual images, of the test pattern. The 30 nm features can be easily distinguished and confirm the elimination of thermal drift blurring by our TXM. Fig. 6(*b*) shows the first and the last of a series of 100

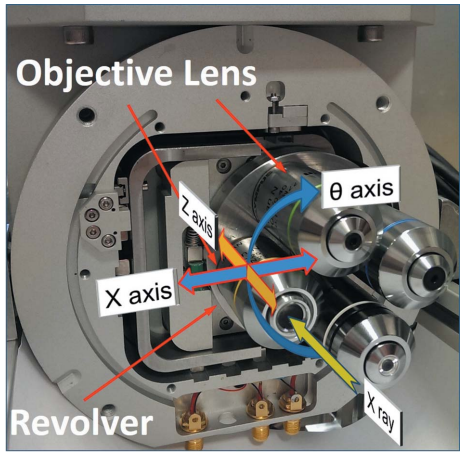

Figure 5
Photograph of the module in the detection system that converts X-rays into visible light. The module includes a revolver lens holder providing different magnifications.

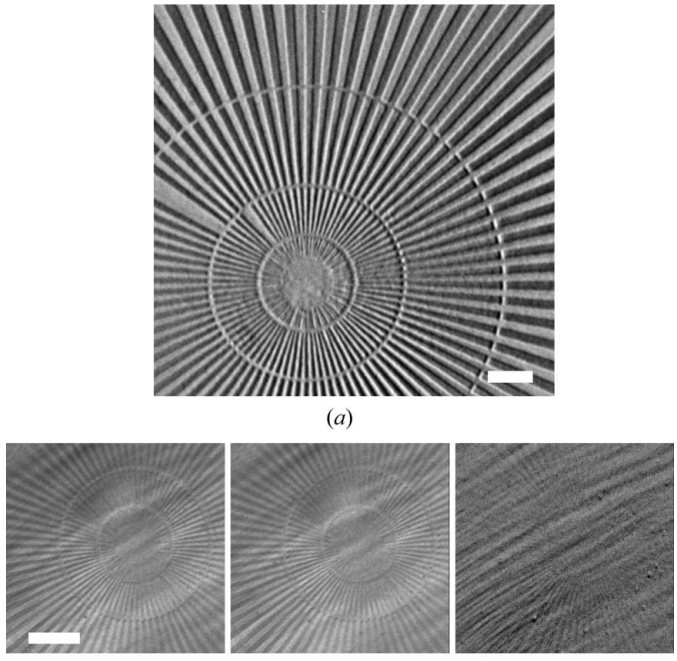

Figure 6
(*a*) Transmission X-ray micrograph of a star test pattern. The features in the innermost region of the pattern are of 30 nm half-period. Next-level features, ~60 nm half-period, are well resolved by our zone plate objectives of 60 nm outermost zones. This is the pixel-by-pixel combination of ten images taken in sequence: the recording time was 20 s per picture corresponding to an overall time of 220 s including storage. Scale bar: 1 μm. (*b*) The individual first and last photograph from a series and the difference image. Scale bar: 2 μm. The artefacts on the edges of line features are due to refraction-related edge enhancements that do not affect our conclusions.

Figure 7
Photograph of TXM modules packaged in a suitcase for transportation.

images taken at different times, ∼60 min in between, and the difference image; they are similar to each other, except the noticeable difference in the background that is probably due to the beam instability. Note, however, that even a very small drift, ∼30 nm in the vertical direction, is already detectable in the difference image, and, without stability at this level, it is unlikely that high-resolution images free from the drift blur can be obtained during single image acquisition. This result corroborates the previous conclusion that our TXM assembled from an individually tested nanopositioning system has made substantial improvement which will be useful in achieving high-resolution images under low lumination conditions.

As far as the easy operation is concerned, Fig. 7 shows the packaging of components for transportation. The optics parts of the TXM can be packed into one suitcase and the imaging module into another, qualifying as check-in luggage. The re-assembly of the components on the beamline can be completed by two or three people in one hour including the pre-alignment. The fine alignment takes from a few hours to a day.

Note that this test was performed in the atmosphere and suffers from air attenuation for the 6.5 keV photon energy. A vacuum version under development will further improve the performance.

The authors would like to thank the personnel of the machine shop of the Institute of Physics, Academia Sinica, for the fabrication of all the mechanical parts of this instrument. This work is supported by the Thematic Project of Academia Sinica and National Nanoscience and Nanotechnology project of the National Science Council.

References

Berujon, S., Wang, H., Pape, I., Sawhney, K., Rutishauser, S. & David, C. (2012). *Opt. Lett.* **37**, 1622–1624.
Chao, W., Fischer, P., Tyliszczak, T., Rekawa, S., Anderson, E. & Naulleau, P. (2012). *Opt. Express*, **20**, 9777–9783.
Chen, T. Y., Chen, Y. T., Wang, C. L., Kempson, I. M., Lee, W. K., Chu, Y. S., Hwu, Y. & Margaritondo, G. (2011). *Opt. Express*, **21**, 19919–19924.
Chen, Y. T., Chen, T. Y., Yi, J., Chu, Y. S., Lee, W. K., Wang, C. L., Kempson, I. M., Hwu, Y., Gajdosik, V. & Margaritondo, G. (2011). *Opt. Lett.* **36**, 1269–1271.
Chen, Y. T., Lo, T. N., Chiu, C. W., Wang, J. Y., Wang, C. L., Liu, C. J., Wu, S. R., Jeng, S. T., Yang, C. C., Shiue, J., Chen, C. H., Hwu, Y., Yin, G. C., Lin, H. M., Je, J. H. & Margaritondo, G. (2008*b*). *J. Synchrotron Rad.* **15**, 170–175.
Chen, Y. T., Lo, T. N., Chu, Y. S., Yi, J., Liu, C. J., Wang, J. Y., Wang, C. L., Chiu, C. W., Hua, T. E., Hwu, Y., Shen, Q., Yin, G. C., Liang, K. S., Lin, H. M., Je, J. H. & Margaritondo, G. (2008*a*). *Nanotechnology*, **19**, 395302.
Chien, C. C., Tseng, P. Y., Chen, H. H., Hua, T. E., Chen, S. T., Chen, Y. Y., Leng, W. H., Wang, C. H., Hwu, Y., Yin, G. C., Liang, K. S., Chen, F. R., Chu, Y. S., Yeh, H. I., Yang, Y. C., Yang, C. S., Je, J. H. & Margaritondo, G. (2013). *Biotechnol. Adv.* **31**, 375–386.
Chubarova, E., Nilsson, D., Lindblom, M., Reinspach, J., Birch, J., Vogt, U., Hertz, H. M. & Holmberg, A. (2011). *Microelectron. Eng.* **88**, 3123–3126.
Chu, Y. S., Yi, J. M., De Carlo, F., Shen, Q., Lee, W. K., Wu, H. J., Wang, C. L., Wang, J. Y., Liu, C. J., Wang, C. H., Wu, S. R., Chien, C. C., Hwu, Y., Tkachuk, A., Yun, W., Feser, M., Liang, K. S., Yang, C. S., Je, J. H. & Margaritondo, G. (2008). *Appl. Phys. Lett.* **92**, 103119.
David, C., Gorelick, S., Rutishauser, S., Krzywinski, J., Vila-Comamala, J., Guzenko, V. A., Bunk, O., Färm, E., Ritala, M., Cammarata, M., Fritz, D. M., Barrett, R., Samoylova, L., Grünert, J. & Sinn, H. (2011). *Sci. Rep.* **1**, 57.
Feng, Y., Feser, M., Lyon, A., Rishton, S., Zeng, X., Chen, S., Sassolini, S. & Yun, W. (2007). *J. Vac. Sci. Technol. B*, **25**, 2004–2007.
Gorelick, S., Vila-Comamala, J., Guzenko, V. A., Barrett, R., Salomé, M. & David, C. (2011). *J. Synchrotron Rad.* **18**, 442–446.
Gorniak, T., Heine, R., Mancuso, A. P., Staier, F., Christophis, C., Pettitt, M. E., Sakdinawat, A., Reusch, R. T., Guerassimova, N., Feldhaus, J., Gutt, C., Grübel, G., Eisebitt, S., Beyer, A., Gölzhäuser, A., Weckert, E., Grunze, M., Vartanyants, I. A. & Rosenhahn, A. (2011). *Opt. Express*, **19**, 11059–11070.
Huang, R. & Bilderback, D. H. (2006). *J. Synchrotron Rad.* **13**, 74–84.
Hwu, E.-T., Nazaretski, E., Chu, Y. S., Chen, H. H., Chen, Y. S. & Hwu, Y. (2013). *Rev. Sci. Instrum.* **84**, 123702.
Kagoshima, Y., Takano, H., Koyamay, T., Tsusaka, Y. & Saikubo, A. (2011). *J. Appl. Phys.* **50**, 022503.
Koyama, T., Takano, H., Konishi, S., Tsuji, T., Takenaka, H., Ichimaru, S., Ohchi, T. & Kagoshima, Y. (2012). *Rev. Sci. Instrum.* **83**, 013795.
Kuwabara, H., Yashiro, W., Harasse, S., Mizutani, H. & Momose, A. (2011). *Appl. Phys. Express*, **4**, 062502.
Lo, T. N., Chen, Y. T., Chiu, C. W., Liu, C. J., Wu, S. R., Lin, I. K., Su, C. I., Chang, W. D., Hwu, Y., Shew, B. Y., Chiang, C. C., Je, J. H. & Margaritondo, G. (2007). *J. Phys. D*, **40**, 3172–3176.
Mayer, M., Grévent, C., Szeghalmi, A., Knez, M., Weigand, M., Rehbein, S., Schneider, G., Baretzky, B. & Schütz, G. (2011). *Ultramicroscopy*, **111**, 1706–1711.
Niedermann, Ph., Emch, R. & Descouts, P. (1988). *Rev. Sci. Instrum.* **59**, 368–369.
Nilsson, D., Uhlén, F., Reinspach, J., Hertz, H. M., Holmberg, A., Sinn, H. & Vogt, U. (2012). *New J. Phys.* **14**, 043010.
Rehbein, S., Guttmann, P., Werner, S. & Schneider, G. (2012). *Opt. Express*, **20**, 5830–5839.
Uhlén, F., Lindqvist, S., Nilsson, D., Reinspach, J., Vogt, U., Hertz, H. M. & Holmberg, A. (2011). *J. Vac. Sci. Technol. B*, **29**, 06FG03.
Wojcik, M., Joshi, J. V., Sumant, A. V., Divan, R., Ocola, L. E., Lu, M. & Mancini, D. C. (2010). *J. Vac. Sci. Technol. B*, **28**, C6P30.
Wu, H. R., Chen, S. T., Chu, Y. S., Conley, R., Bouet, N., Chien, C. C., Chen, H. H., Lin, C. H., Tung, H. T., Chen, Y. S., Margaritondo, G., Je, J. H. & Hwu, Y. (2012). *J. Phys. D*, **45**, 242001.
Wu, S.-R., Hwu, Y. & Margaritondo, G. (2012). *Materials*, **5**, 1752–1773.
Yin, G. C., Song, Y. F., Tang, M. T., Chen, F. R., Liang, K. S., Duewer, F. W., Feser, M., Yun, W. B. & Shieh, H. P. D. (2006). *Appl. Phys. Lett.* **89**, 221122.